Path-integral computations of tunneling processes

Ilan Benjamin
Department of Chemistry, University of California, Santa Cruz, California 95064

Abraham Nitzan[a)]
School of Chemistry, The Sackler Faculty of Exact Sciences, Tel Aviv University, Tel Aviv 69978, Israel

(Received 21 March 2005; accepted 2 June 2005; published online 14 September 2005)

The application of the path-integral methodology of Chandler and Wolynes [D. Chandler and P. G. Wolynes, J. Chem. Phys. **74**, 4078 (1981)] to the calculation of one-electron-tunneling probabilities is revisited. We show that the evaluation of the kink free energy that is related to the tunneling splitting is associated with "polymer bead" distributions over a continuous distribution of scaled barriers, which makes both the calculation and its physical interpretation relatively difficult. In particular, we find that relative to other available techniques the method converges slowly and suffers from inaccuracies associated with the finite-temperature aspect of the calculation, and that past tentative identification of the bead distribution over the barrier with a physical picture of a "tunneling path" should be reassessed. © *2005 American Institute of Physics*.
[DOI: 10.1063/1.2036989]

I. INTRODUCTION

Numerical simulations of electron transfer reactions broadly fall into three categories. One class of calculations relies on the Marcus conceptual picture[1] and attempts to extract information about the relevant free-energy surfaces and the activation and reorganization energies from a microscopic model. Another seeks to describe solvent dynamical effects in electron transfer reactions, usually by addressing numerically spin-boson-type problems. Finally, again within the Marcus conceptual picture, one needs to evaluate the electronic tunneling probability or, rather, the electronic coupling between the donor and the acceptor. At issue is the solvent effect on this tunneling matrix element and its dependence on the electron energy and on the donor-acceptor distance. A closely related issue is the characterization of the *tunneling path* or the distribution of tunneling paths. While not directly observable, knowledge about the likelihood of finding the electron along different paths in the tunneling barrier is useful both for its bearing on our understanding of the tunneling process and on the ability to control the tunneling current. The latter issue is of potential importance in electronic transport in nanojunctions. Another useful concept is the *effective barrier height*—the rectangular barrier of width equal to the donor-acceptor distance that will give the same tunneling probability as the actual one.

As a computational task this problem is usually handled as a tunneling probability through a complicated three-dimensional potential barrier which is roughly determined by the ionization energies of the donor and acceptor species (containing the "extra" electron) superimposed with the electron-solvent interaction. In many cases the energetics is such that the process can be described within the atomic-orbital basis sets used in standard quantum chemistry calculations. Such an approach has been extensively used to describe electron transfer in proteins.[2] Alternatively, if an appropriate semiempirical pseudopotential for the electron-solvent interaction is available, the process may be described as a one-electron tunneling in the complicated potential landscape comprising the donor, the acceptor, and this pseudopotential. This approach was used recently to describe processes involving excess electrons in water, alcohols, and ammonia environments. In a recent series of articles[3–6] we have used the latter approach to investigate electron tunneling through water barriers, focusing on the effect of the water environment on the tunneling process, and have found that electron tunneling through a water layer is very sensitive to the three-dimensional structure of the water layer. These calculations were done on numerical grids using the absorption boundary conditions Green function (ABCGF) methodology.

An alternative approach to tunneling probabilities through complex environments given an electron-solvent pseudopotential is based on the path-integral methodology of Chandler and co-workers[7,8] and Kuki and Wolynes.[9] For the transfer between the lowest-lying local donor and acceptor states $[\psi_1(\mathbf{r}) \equiv |1\rangle, \psi_2(\mathbf{r}) \equiv |2\rangle]$, one focuses on matrix elements of the imaginary time propagation

$$I_{12} = \langle 1|e^{-\beta H}|2\rangle = \int d\mathbf{r}_i \psi_1(\mathbf{r}_i) \int d\mathbf{r}_f \psi_2(\mathbf{r}_f) \int_{\mathbf{r}_i}^{\mathbf{r}_f} \mathcal{D}\mathbf{r}(\beta) \times \exp\left\{ -\int_0^\beta H(\mathbf{r}(\beta'))d\beta' \right\} \quad (1)$$

and the equivalent I_{11}, where $H(\mathbf{r}(\beta)) = (m/2)(d\mathbf{r}/d\beta)^2 + V(\mathbf{r}(\beta))$ and $V(\mathbf{r})$ is the potential on which the electron moves. The symbol $\mathcal{D}$ denotes path integration, here with fixed initial and final points $\mathbf{r}_i$ and $\mathbf{r}_f$. An approximation to the path integral is obtained by cutting the path to P segments at corresponding intervals β/P. This leads to an expression in the form of the partition function of a harmonic

[a)]Electronic mail: nitzan@post.tau.ac.il

polymer chain with $P+1$ beads, fixed at the initial ($\mathbf{r}_0=\mathbf{r}_i$) and final ($\mathbf{r}_P=\mathbf{r}_f$) positions,

$$\int_{\mathbf{r}_i}^{\mathbf{r}_f} \mathcal{D}\mathbf{r}(\beta)\exp\left\{-\int_0^\beta H(\mathbf{r}(\beta')d\beta')\right\} = \int d\mathbf{r}_1 \int d\mathbf{r}_2 \ldots \int d\mathbf{r}_{P-1}\left(\frac{m}{2\pi\hbar^2\beta/P}\right)^{3P/2} \times\exp\left[-\left(\frac{\beta}{P}\right)\sum_{i=1}^{p}\left(\frac{m(\mathbf{r}_i-\mathbf{r}_{i-1})^2}{2(\hbar\beta/P)^2}+V(\mathbf{r}_i)\right)\right]. \quad (2)$$

An important result for deep tunneling (high tunneling barrier) in symmetric structures is that the tunneling splitting Δ is related to the free energy F_K of forming a single kink in the structure of this polymer chain at the temperature $T=(k_B\beta)^{-1}$. A kink is defined as a segment of the polymer chain that goes between the two wells, and F_K is the free-energy difference between two structures of the harmonic bead chain: one in which $\mathbf{r}_i$, $\mathbf{r}_f$, and all connecting beads stay in the initial well and the other where $\mathbf{r}_i$ and $\mathbf{r}_f$ are restricted to be on opposite wells with only one kink connecting the two wells. The tunneling splitting, which provides a measure for the electronic coupling, is given by[9]

$$\Delta = \beta^{-1}e^{-\beta F_K} \quad (3)$$

provided that $\Delta \ll \beta^{-1} \ll \Delta E$, where ΔE is the spacing between the split levels and higher quantum states. For completeness, a proof of Eq. (3) is given in Appendix A. We note in passing that another path-integral approach, using approximations based on the path centroid density,[10] may be useful for describing tunneling effects at higher temperatures and in dissipative environments. Equations (2) and (3) provide a route for computing F_K and thus Δ by classical free-energy computation methods based, e.g., on the Monte Carlo procedure. An application to electron transfer between Fe^{+2} and Fe^{+3} in water was described in Ref. 8. Furthermore, Kuki and Wolynes[9] have made the appealing suggestion that the distribution of paths that contribute to F_K can provide additional information on the route taken by the tunneling particle through the solvent structure and have explored this idea for electron transfer in proteins.

In this paper we revisit this problem in an attempt to examine the viability and usefulness of this method in comparison with the ABCGF methods used in our earlier calculations. To this end we investigate two systems. In one the electron tunnels through a simple rectangular potential. In the other tunneling occurs through a static layer of water molecules sampled from a thermal distribution of water configurations. We carry out numerical studies similar to that of Kuki and Wolynes for electron transfer in these model systems and at the same time examine critically the foundation of their assumption that the distribution of paths contributes to the path integral (2). We find that the method is tractable; the needed free energy can be expressed as an integral over an averaged potential-weighted sum over the polymer beads that occupy the barrier, and the distribution of kink trajectories qualitatively reflects the distribution of tunneling paths. However, the procedure converges relatively slowly and detailed insight is obscured by the fact that kink configurations from infinitely many scaled barriers contribute to the overall tunneling probability. We note that while these observations suggest that this method for calculating tunneling probabilities in static configurations is of limited value, path-integral methodology provides a principal route for evaluating tunneling probabilities of particles interacting with their thermal environment and with each other.

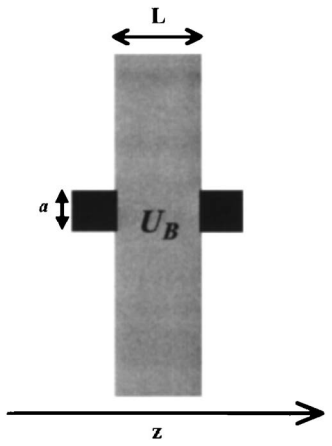

FIG. 1. The basic model used in the calculation. The gray area that represents the potential barrier $U_B(\mathbf{r})$ is a slab of thickness L in the tunneling (z) direction infinite in the x-y plane. Outside the slab the potential is taken infinite anywhere, except with the cubic volumes of linear size a, denoted by the black squares, where the potential is taken to be zero [i.e., $U_B(\mathbf{r})$ measures the height of the potential barrier above the bottom of these wells].

II. MODEL

Since we are interested in assessing the usefulness of the method rather than in a specific calculation, we have chosen a model that reflects our interest in electron transmission probabilities through molecular layers. Such transmission processes do not involve donor and acceptor species and are best viewed as scattering processes in which the initial energy of the tunneling particle is well defined. Furthermore, the barrier used to describe such processes should mimic a molecular layer: infinite in two directions (x and y, say) and finite with thickness L in the transmission direction z. The path-integral method described above and in Appendix A relies on a picture of two localized states separated by a barrier. We have therefore chosen to consider tunneling in a model described in Fig. 1. The slab represents the molecular layer. The wells, however, are artificial constructs. They are chosen to be deep and narrow enough so that the ground state in the corresponding isolated well (a limit obtained when the slab is infinitely wide) is well separated (relative to k_BT) from the lowest excited state. This ground-state energy then defines the initial energy for the tunneling calculation.

This choice of a particular model raises a question concerning the generality of the results obtained. At issue is to what extent the tunneling probability calculated is a property of the barrier and of the initial energy, and how much of it reflects specific properties of the initial and final states. Recall that tunneling may be described by a coupling term in the Hamiltonian when represented in a basis of states localized on the two sides of the barrier.[11] In one dimension this effective coupling between the local states in the well is de-

rived from their overlap in the barrier, which primarily depends on their energy. In a three-dimensional system the total energy does not uniquely determine the overlap: in a separable problem it would be determined by the energy in the z direction. For a deep enough cubic well this energy is roughly 1/3 of the total ground-state energy. We have verified (see below) that for such wells of different dimensions but with the same ground-state energy (obtained from varying both the well depth and its width), the path-integral results are very similar.

III. THE KINK FREE ENERGY AND THE TUNNELING PROBABILITY

For definiteness we consider the path integral (2) where x_i is located on one well and compare two cases, one where x_f is located in the same well, the other where it is located in the opposite well, a distance L apart. We are thus interested in the corresponding two configurations of the polymer chain. The free-energy difference between these configurations can be represented as a sum

$$F_K = F_K^{(1)} + F_K^{(2)}, \tag{4}$$

where $F_K^{(1)}$ is the free energy needed to stretch the polymer chain in free space, i.e., to move the restricted position of the last bead from the position identical to that of the first bead to another position at distance L in the absence of a potential. $F_K^{(2)}$ is the free-energy difference between the resulting stretched configuration in free space and another configuration obtained when a potential barrier is introduced while keeping the first and last beads pinned to their positions on the opposite sides of the barrier, a distance L from each other. Obviously, the components $F_K^{(i)}$, $i=1,2$, have no physical significance and other decompositions of the kink free energy could be used to facilitate computation.

In Appendix B we show that four our polymer chain in free space the partition function, Eq. (2), evaluated under the restriction $\mathbf{r}_0=0$, $|\mathbf{r}_N|=d$ yields

$$Z_1(d) = A_0 \exp(-md^2/(2\hbar^2\beta)), \tag{5}$$

where A_0 is a constant. The free energy to stretch the polymer to a distance L between the first and last bead is therefore

$$F_K^{(1)}(L) = -k_B T \ln\left(\frac{Z_1(L)}{Z_1(0)}\right) = (k_B T)^2 mL^2/(2\hbar^2). \tag{6}$$

Interestingly, this free energy increases as T^2. It should be noted that Eq. (6) is an approximation: it is based on a free-space calculation and disregards the fact that our system is confined to the volume defined by the slab and the two cubic regions in Fig. 1. The order of magnitude of this contribution to the free energy is $k_B T f$, where f is the ratio $k_B T/\varepsilon$ and ε is of the order of the ground-state energy of the tunneling particle in a one-dimensional rectangular infinitely deep box of width L. For L of the order of 10 Å and $T=300$ K, $f \ll 1$ and $f_K^{(1)} \ll k_B T$. We will see that this contribution to the free energy may be altogether disregarded relative to $F_K^{(2)}$.

Appendix B also describes the procedure for calculating $F_K^{(2)}$. The result can be expressed in terms of the average density $\langle \rho(\mathbf{r}) \rangle_\lambda$ of beads on the scaled barrier $\lambda V(\mathbf{r})$

$$F_K^{(2)} = \frac{1}{P} \int d\mathbf{r} V(\mathbf{r}) \int_0^1 d\lambda \langle \rho(\mathbf{r}) \rangle_\lambda, \quad P \to \infty. \tag{7}$$

Since ρ is expected to be linear in the number of beads P, the result does not depend on this number, as is verified below. For a rectangular barrier, $V(\mathbf{r})=U_B$ on the barrier and zero otherwise, Eq. (7) yields

$$F_K^{(2)} = \frac{U_B}{P} \int_0^1 d\lambda \langle n_b \rangle_\lambda, \tag{8}$$

where $\langle n_b \rangle_\lambda$ is the average number of beads on a barrier of height λU_B above the bottom of the side wells. For $U_B \gg k_B T$, $F_K^{(2)}$ is seen to dominate the kink free energy. Either (7) or (8) can be easily computed within the same simulation of the path integral (2).

The observation that $F_K^{(2)}$ is related to the distribution of beads on the barrier supports the intuitive notion taken in Ref. 9 that this distribution is somehow related to the tunneling path. Equation (8), however, indicates that one should be careful about this interpretation since *the integral over* λ *contains contributions from bead distributions associated with all scaled potentials* $\lambda V(\mathbf{r})$. Some characteristics of such distributions are shown as functions of λ below.

IV. RESULTS OF MODEL CALCULATIONS

In order to gain insight about the nature of the path-integral calculation and the significance of the computed configurations and their distribution, we have performed several calculations of electron tunneling in the simple configuration of Fig. 1 using a rectangular barrier of width $L=10$ Å and two identical wells placed opposite each other. The equilibration of the system and the production of equilibrium configurations were done by a Monte Carlo (MC) procedure using chains of at least a thousand beads, with the end beads taken fixed on the opposite sides of the barrier, in the center of the side wells. In some cases the number of beads P was varied in order to check the convergence of the calculation as well as to validate the integrity of the measures used to compare the paths in the different systems studied. We have focused on two such measures: the fraction of beads that occupy the barrier region that is related to the tunneling splitting, and the lateral width of the bead distribution on the barrier. In the range of bead numbers that were used in these calculations we did not observe more than one kink in the sampled configurations.

In the Monte Carlo evolution a move is attempted on each bead in its turn and is accepted or rejected using the usual energy criterion based on the potential that appears in the exponent of Eq. (2). Typically, 200 000 configurations of the polymer chain were sampled at intervals of 20 cycles apart (in a cycle one move is attempted for each bead). For each system studied an equilibration stage has to precede the production run. During the equilibration we have used a variable MC step size adjusted to yield approximately 40% ac-

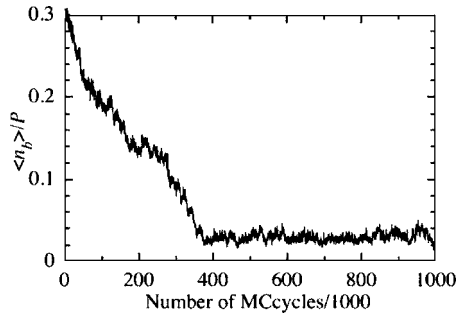

FIG. 2. Convergence of a typical equilibration run for a polymer chain ($P=2000$) across a rectangular slab (Fig. 1). The figure shows the evolution of the average number of beads in the barrier region with the number of MC cycles. The parameters used are $U_B=15$ eV, $a=3$ Å, and $T=300$ K. The ground-state energy in an isolated well of size $3\times3\times3$ Å^3 surrounded by infinite walls on five sides and by a wall of height 15 eV on one side is approximately 11.6 eV, i.e., about 3.4 eV below the top of the barrier.

ceptance ratio. In the production stage the MC step size was kept fixed, at the value assumed at the end of the equilibration. The configurations sampled during the production run were used to analyze the path, as described below.

Our main interest lies in correlating the path characteristics with the barrier structure and energetics. To this end the choice of the side wells should not make an essential difference, except by fixing the energy. Indeed we have verified that using $a=3$ Å and $U_B=20$ eV ($U_B-E_g\sim8.4$ eV), $a=4$ Å and $U_B=15$ eV ($U_B-E_g\sim8.5$ eV) gave the same fraction, 0.02 ($\pm5\%$) of beads in the (rectangular) barrier region.

The convergence of these calculations is rather slow; Fig. 2 shows a typical equilibration behavior in a simulation of tunneling in the configuration of Fig. 1 using $P=2000$ beads. Shown is the calculated fraction $\langle n_b \rangle / P$ of beads on the barrier as a function of the number of MC steps. In this run nearly 400 000 MC cycles (steps per bead) were needed to equilibrate the polymer chain. It should be noted, however, that in calculations that study the dependence of tunneling on system parameters much of the efforts involved in the equilibration can be saved by starting each run from equilibrated configurations obtained from neighboring parameter values.

Figure 3 shows some characteristics of the converged equilibrium distribution $P(n_b)$ of the number of beads in the barrier region. The distribution itself is shown in Fig. 3(a) for different total numbers of beads P. The distribution is rather broad and the corresponding average $\langle n_b \rangle$ and the width $\sigma=(\langle n_b^2 \rangle - \langle n_b \rangle^2)^{1/2}$ are proportional to P. This is seen explicitly in Figs. 3(b) and 3(c). The inset to Fig. 3(a) shows the same data expressed as the distribution of fraction of beads, $P(x)$, $x=n_b/P$. Here the different distributions collapse to a single one, as expected. We thus verify that the numbers $\langle n_b \rangle / P$ and σ/P behave, as expected, as characteristics of the tunneling process that do not depend on the number of beads used in the calculation.

The results shown in Fig. 4 focus on bead distributions obtained from different scaled potentials. The barrier/well parameters are $a=3$ Å and $U_B=15$ eV and results are shown at temperatures 200 and 300 K. 1000 beads are used in this calculation and 2×10^5 configurations sampled at 20-cycle

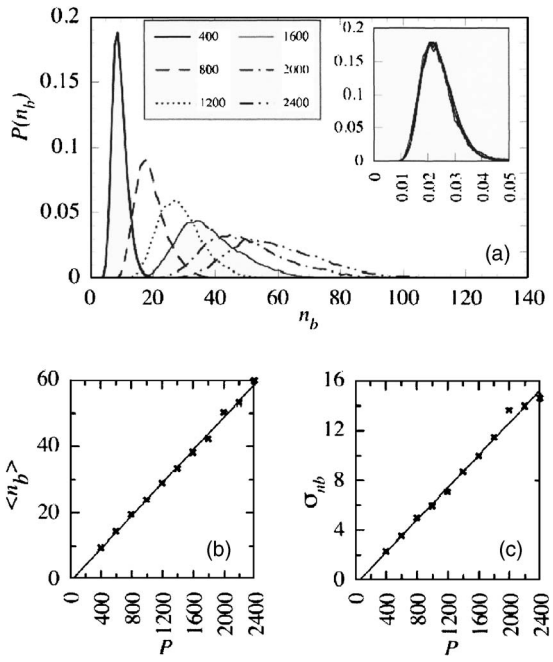

FIG. 3. (a) The distribution $P(n_b)$ of the number of beads in the barrier region, obtained from calculations using different numbers of beads on a rectangular barrier (Fig. 1) with the same parameters as in Fig. 2. The inset shows the same data expressed as the distribution of $x=n_b/P$. These results were compiled from the result of the 10^6 path-integral Monte Carlo cycles following an equilibration run of 10^6 cycles. (b) The average number of beads in the barrier region $\langle n_b \rangle$ obtained from the calculation done for Fig. 3(a), displayed as a function of the total number of beads P. (c) The width of the bead distribution, $\sigma=(\langle n_b^2 \rangle - \langle n_b \rangle^2)^{1/2}$, plotted as a function of P obtained from the simulations of Fig. 3(a).

intervals were used for each scaling parameter λ. For a given λ the calculations are done using the scaled barrier λU_B. Shown as functions of λ are the average bead number $\langle n_b \rangle$ and the average gyration radius of the bead distribution on

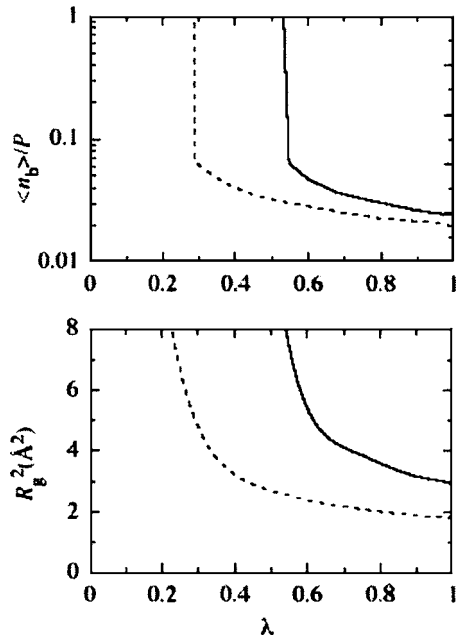

FIG. 4. Upper panel: the fraction n_b/P. Lower panel: The gyration radius R_g plotted against the scaling factor λ. Parameters are as in Fig. 2. Full line: $T=300$ K. Dotted line: $T=200$ K.

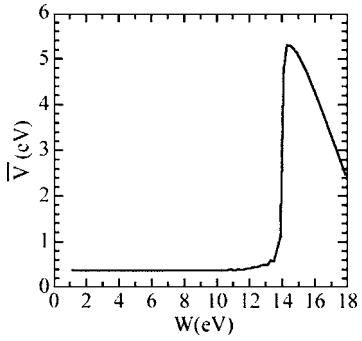

FIG. 5. $\bar{V}=P^{-1}\Sigma_i V(\mathbf{r}_i)$ (sum over all beads on the barrier) displayed against the depth W of the middle well, expressed as a height above the bottom of the side wells. The barrier height above this bottom is $U_B=20$ eV. The side-well dimensions are $a\times a\times a$, $a=3$ Å. The overall barrier width is $L=10$ Å and the dimensions of the central well are $b\times b\times b$ with $b=6$ Å.

the barrier, $R_g=n_b^{-1}\Sigma_{i\in n_B}(x_i^2+y_i^2)^{1/2}$, where x_i and y_i measure the lateral distances of the beads on the barrier from the line that connects the centers of the two wells. We find that both behave almost as step functions, for example, $\langle n_b\rangle/P$ drops from its free space value, essentially 1, to 0.1 on a very narrow λ interval above a critical value λ_c that depends on the temperature. The desired free energy is essentially the area below the $\langle n_b\rangle$ line. This implies, according to Eq. (8), that approximately $F_K^{(2)}=\lambda_c(T)U_B$.

An important class of tunneling transport phenomena include those that involve resonance tunneling. It is of interest to observe such tunneling processes in the context of the path-integral formulation. In Fig. 5 we examine the behavior of the bead distribution associated with the path integral (2) for a rectangular barrier in which a cubic rectangular well is placed in the middle of the barrier along the line connecting the two side wells (see inset to Fig. 5). The barrier width is, as before, $L=10$ Å and the width of the middle cubic well is $b=6$ Å. The other parameters are, again as before, $a=3$ Å, $U_B=20$ eV, and $T=300$ K. The number of beads used is 1000. We vary the depth W of the middle well in order to change the energy of its ground state. Resonance conditions occur, and the tunneling probability peaks, when the energies of the state in the side well and in the middle well coincide. A full calculation of the tunneling probability requires the computation for each value of W of $\bar{V}(\lambda)=P^{-1}\int d\mathbf{r}V(\mathbf{r})\times\langle\rho(\mathbf{r})\rangle_\lambda$ for each λ, then integrating the result over all λ. We did not attempt this time-consuming calculation here. Instead we shown in Fig. 5 how resonance tunneling manifests itself in the calculation of the integrand $\bar{V}$ at one particular point, $\lambda=1$. The signature of the resonance state is seen as a strong peak in the dependence of $\bar{V}$ on W, however, it needs to be emphasized that the shape and position of this structure do not reflect the tunneling resonance that can be obtained using (3) only from the full calculation of F.

Finally, we examine the application of such path-integral calculation for electron tunneling through a water barrier. Water configurations were prepared as described in Ref. 5. Briefly, classical room-temperature equilibrium molecular-dynamics (MD) simulations were run for water layers between Pt electrodes and the configurations used in the present analysis were sampled from the equilibrium trajectory. The results shown in Figs. 6 and 7 were obtained from configurations that have three water monolayers between the two metal surfaces (barrier width $\sim$10 Å). The electron-water interaction is the pseudopotential constructed by Rossky and Schnitker,[12] supplemented to include the effect of water electronic polarizability as described in Refs. 3 and 5. We have also used an artificial repulsive electron-water potential that is obtained from the "real" one by setting the electron charge to zero (thus eliminating all electrostatic interactions, leaving only short-range repulsive terms). Comparing between the behavior of the tunneling processes under this repulsive potential and the real one enables us to examine the effect of the water spacer on the electron-tunneling process against a repulsive barrier of the same structure—essentially to study the balance between the effect of the repulsive oxygen cores and the attractive polarizability response in determining the tunneling probability. The overall barrier potential is taken as a superposition of the electron-water pseudopotential and a rectangular barrier, whose height above the ground-state energy of the electrons in the side wells represents the work function of the metal electrodes.

The first statement that should be made about the application of this path-integral technique to the evaluation of tunneling characteristics of the electron-water system is that it is, in many respects, not competitive with other available methods, in particular, the absorbing boundary condition Green's function methodology that we have applied before. In particular, combining a numerical grid-based calculation of the Green function with an exact evaluation of energy-dependent absorbing boundary potential (i.e., self-energy) makes the latter a highly efficient and accurate method.[6,13] Still, in view of past interest in the path-integral approach to tunneling calculations, it is interesting also to examine this method with regard to electron tunneling in water. We note in passing that path-integral methodology is expected to have a much better scaling with the number of particles involved in the tunneling process than any method based on a grid representation of the quantum-mechanical wave function.

Figures 6 and 7 show results obtained from these calculations. Because this approach is highly CPU intensive, we have limited our study to two issues. Figure 6 shows result pertaining to the effective barrier potential. Shown as a function of λ is the average potential $\bar{V}(\lambda)=P^{-1}\int d\mathbf{r}\langle\rho(\mathbf{r})\rangle_\lambda V(\mathbf{r})$ that determines the free energy $F_K^{(2)}$ via Eq. (7). This potential is plotted against λ for the full electron-water pseudopotential (dotted line), the repulsive electron-water interaction (dashed line), and for the vacuum barrier. The qualitative behavior of these potentials is similar to what was found in our earlier calculations using the ABCGF method.[3,5] the presence of water in the barrier lowers the effective barrier height relative to vacuum, while, not surprisingly, the repulsive "water" increases the effective barrier height. We have found, however, that from quantitative comparison between these models this method performs poorly because for $\lambda<0.5$, even with our relatively large sampling size (see Sec. IV), the statistical fluctuations were bigger than the difference between the models. This problematic character of the

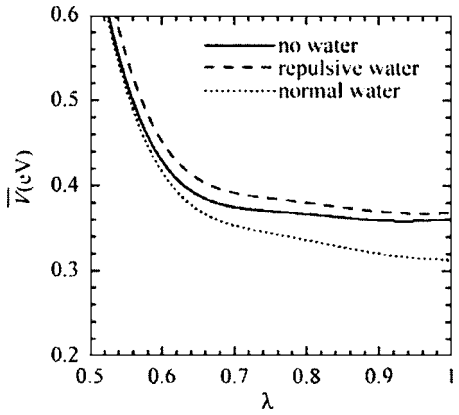

FIG. 6. $\bar{V}(\lambda)=P^{-1}\int d\mathbf{r}\langle\rho(\mathbf{r})\rangle_\lambda V(\mathbf{r})$ displayed as a function of λ for a potential barrier made of three monolayers of water molecules (width ~10 Å). The overall potential is taken to be $V(\mathbf{r})=U_B+V_{\text{el-water}}(\mathbf{r})=15$ eV $+V_{\text{el-water}}(\mathbf{r})$ above the bottom of the side wells. The calculation is done at $T=300$ K.

path-integral calculations can be understood by noting that Eqs. (3) and (7) imply that fluctuations of the order of $\sim k_BT$ in $\bar{V}$ amount to uncertainty of the order of e in the tunneling probability so the transmission probability can be determined only within a factor of this order. (Our earlier results[3,5] gave a factor of ~5 between the tunneling probability in vacuum and in water for a barrier width ~10 Å). We have also attempted to run the path-integral simulations at lower temperatures (100 K), but found that convergence in this case was impractically slow.

Figure 7 shows the distribution of polymer beads of a typical kink across the water barrier (made of three water monolayers) in relation to the distributions of water molecules in the barrier. This result is equivalent to Fig. 1 of Ref. 9 that was suggested to reflect the electron-tunneling path. Shown is a two-dimensional projection on a plane parallel to the tunneling direction, where the black dots mark the centers of the water oxygen atoms and the open circles are the polymer beads. Two features are evident. First, the beads prefer to accumulate near the water layers, again reflecting the attractive nature of water that leads to the lowering of the effective barrier. Second, the kink connects the initial and final wells with what appears to be a straight line in the tunneling direction, with only small fluctuations about this direction. Indeed we have obtained similar results from 20 independent water configurations, and averaging over many kinks just smears the bead structure in Fig. 7 into a relatively narrow cylinder.

This latter feature stands in contrast to our earlier observations,[6] where the electron-tunneling function was used to obtain the spatial dependence of the tunneling flux according to $\mathbf{J}(\mathbf{r})=\hbar(2mi)^{-1}(\psi^*\nabla\psi-\psi\nabla\psi^*)$. In that work we have identified three distinct situations, with one corresponding to what might be called "straight path tunneling." In the other two the flux distribution is very different from the straight line.

This observation again points to the shortcoming of using the bead distribution in the path-integral calculation as an indicator of the tunneling path. We have already found that the tunneling probability is determined by the bead distributions in kinks obtained for a series of scaled barriers via Eqs. (3) and (7). The bead distribution obtained for a full barrier $V(\mathbf{r})$ is very reasonable for such a high barrier, but obviously not the only and possibly not the most relevant one. Indeed, Fig. 6 shows that $\bar{V}(\lambda)$ increases with decreasing λ, indicating that a scaled barrier with a small λ may dominate the bead distribution associated with the actual tunneling path. For comparison we show in Fig. 7(b) the bead distribution obtained for a scaled barrier, with $\lambda=0.2$.

V. CONCLUSIONS

We have critically examined the application of the technique based on the path-integral methodology of Chandler and co-workers[7,8] and Kuki and Wolynes[9] for evaluating tunneling integrals in condensed phases. Path integrals are among the methods of choice for calculations involving many quantum particles that interact with a classical environment. For single-electron tunneling in the absence of thermal interactions, we have found that this approach suffers from high CPU demand and slow convergence. Physical interpretations based on the spatial distributions of classical beads, while intuitively appealing, are also limited by the fact that contributions to the tunneling probability are associated with the polymer bead distributions on many scaled barrier potentials. Such distributions, in themselves, do not seem the have any particular physical significance. In particular, the bead distribution obtained on the real potential barrier, while certainly related to the tunneling process, cannot be directly identified with a tunneling path distribution.

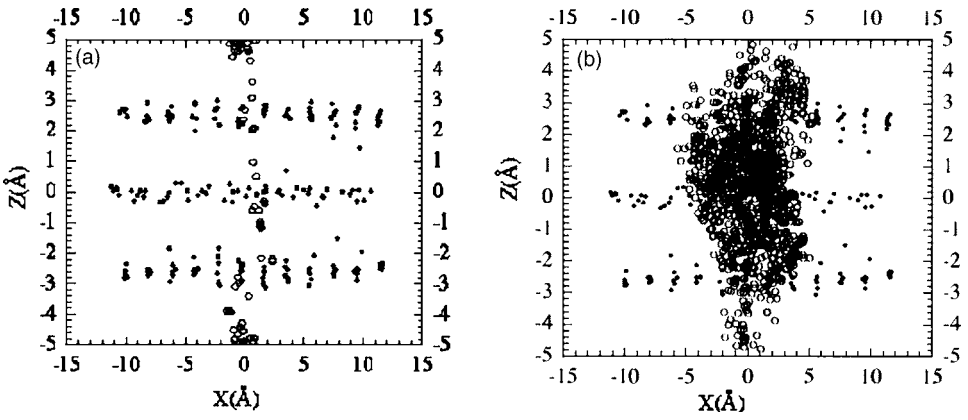

FIG. 7. A two-dimensional projection of a typical polymer kink showing the distribution of beads (open circles) in relation to the positions of the water oxygen atoms (black dots). (a) Full barrier ($\lambda=1$). (b) Scaled barrier ($\lambda=0.2$).

ACKNOWLEDGMENTS

This research was supported by the US-Israel Binational Science Foundation, by the Israel Science Foundation (AN), and by a grant from the National Science Foundation (CHE-0345361, IB).

APPENDIX A: PROOF OF EQ. (3)

Here we provide a simple proof of Eq. (3). In addition, we show that for the path integral associated with the tunneling transition between the two wells separated by a high barrier as in Fig. 1, it is sufficient to restrict the polymer chain to start in one well and end in the other—the exact initial and final positions are not important.

We consider a symmetric double well system. The ground states of the isolated wells are denoted $|1\rangle$ and $|2\rangle$ with energy E_0. Let

$$\Delta \ll \beta^{-1} \ll \Delta E, \tag{A1}$$

where Δ is the tunnel splitting and ΔE is the energy difference between the ground and excited states of the isolated single well. Denote the lowest eigenstates of H by $|+\rangle$ and $|-\rangle$. To a good approximation (exact if there were only one state in each well)

$$|1\rangle = \frac{1}{\sqrt{2}}(|+\rangle + |-\rangle), \quad |2\rangle = \frac{1}{\sqrt{2}}(|+\rangle - |-\rangle). \tag{A2}$$

Therefore, $e^{-\beta H}|1\rangle = 2^{-1/2}(e^{-\beta E_+}|+\rangle + e^{-\beta E_-}|-\rangle)$ and

$$I_{11} = \langle 1|e^{-\beta H}|1\rangle = \frac{1}{2}(e^{-\beta E_+} + e^{-\beta E_-})$$

$$= \frac{1}{2}e^{-\beta E_0}(e^{(1/2)\beta\Delta} + e^{-(1/2)\beta\Delta}), \tag{A3}$$

$$I_{21} = \langle 2|e^{-\beta H}|1\rangle = \frac{1}{2}(e^{-\beta E_+} - e^{-\beta E_-})$$

$$= \frac{1}{2}e^{-\beta E_0}(e^{(1/2)\beta\Delta} - e^{-(1/2)\beta\Delta}). \tag{A4}$$

Using (A1) we have

$$\frac{I_{21}}{I_{11}} = \beta\Delta, \tag{A5}$$

so that

$$-\beta F_K = \ln\left(\frac{I_{21}}{I_{11}}\right) = \ln(\beta\Delta), \tag{A6}$$

which leads immediately to (3). Obviously, at the low temperature considered I_{21} and I_{11} are dominated by single kink and no kink trajectories. This identifies the free energy in (A6) as the free energy to form a single kink.

Note that if instead of states $|1\rangle$ and $|2\rangle$ we take any positions $|x_1\rangle$ in well 1 and $|x_2\rangle$ in well 2, the result would have been the same, because under condition (A1) $e^{-\beta H}|x_1\rangle \simeq \psi_1^*(x_1)e^{-\beta H}|1\rangle$. Instead of (A3) and (A4) we have in this case

$$I'_{11} = \langle x_1|e^{-\beta H}|x_1\rangle = |\psi_1(x_1)|^2 I_{11}, \tag{A7}$$

$$I'_{21}\langle x_2|e^{-\beta H}|x_1\rangle = \psi_2(x_2)\psi_1^*(x_1)I_{21}, \tag{A8}$$

where x_1 and x_2 are positioned in the opposite wells. This leads to

$$-\beta F'_K \equiv \ln\frac{I'_{21}}{I'_{11}} = \ln\left(\frac{\psi_2(x_2)}{\psi_1(x_1)}\right) + \ln(\beta\Delta). \tag{A9}$$

Note that ψ_1 as a ground-state wave function does not have nodes. In the case considered here, $F_K \gg \beta^1$, the terms containing the wave functions can be disregarded.

APPENDIX B: AN ANALYTICAL EXPRESSION FOR THE KINK FREE ENERGY

The kink free energy F_K was defined as the free-energy difference between two polymer configurations. In one, the initial and final beads are restricted to be in one well. In the other, each is restricted to be in a different well, a distance d apart. It can be represented by

$$F_K = F_K^{(1)} + F_K^{(2)}, \tag{B1}$$

where $F_K^{(1)}$ is the free energy to move the restricted position of the last bead from the position identical to that of the first bead to another position at distance d in the absence of a potential. $F_K^{(2)}$ will be the free-energy difference between the resulting configuration (no potential) and the one obtained when the barrier is introduced.

1. Calculation of $F_K^{(1)}$

From Eq. (2)

$$Z_1(d) = \left(\frac{mP}{2\pi\hbar^2\beta}\right)^{3P/2} \int d\mathbf{r}_1 \int d\mathbf{r}_2 \cdots \int d\mathbf{r}_{P-1} \times \exp\left[-\left(\frac{\beta}{P}\right)\sum_{i=1}^{P} \frac{m(\mathbf{r}_i - \mathbf{r}_{i-1})^2}{2(\hbar\beta/P)^2}\right]$$

$$= A \int d\mathbf{r}_1 \int d\mathbf{r}_2 \cdots \int d\mathbf{r}_{P-1} \times \exp\left[-B\sum_{i=1}^{P} (\mathbf{r}_i - \mathbf{r}_{i-1})^2\right], \tag{B2}$$

where

$$A = \left(\frac{mP}{2\pi\hbar^2\beta}\right)^{3P/2}, \quad B = \frac{Pm}{2\hbar^2\beta} \tag{B3}$$

and where

$$\mathbf{r}_0 = 0, \quad |\mathbf{r}_N| = d. \tag{B4}$$

The direction of $\mathbf{r}_N$ should not matter. Once (B2) is evaluated we have

$$F_K^{(1)}(d) = -k_B T \ln\left(\frac{Z_1(d)}{Z_1(0)}\right). \tag{B5}$$

To evaluate (B2) take $P = 2^N$ (the total number of beads is $P+1$, an odd number) and denote the partition function (B2) $Z_1(d;A,B,N)$. Next integrate over the 2^{N-1} variables $\mathbf{r}_1, \mathbf{r}_3, \ldots, \mathbf{r}_{P-1}$. Using

$$\int d\mathbf{r}_1 e^{-B[(\mathbf{r}_1-\mathbf{r}_0)^2+(\mathbf{r}_2-\mathbf{r}_1)^2]}=\left(\frac{\pi}{2B}\right)^{3/2}e^{-(1/2)B(\mathbf{r}_2-\mathbf{r}_0)^2} \quad \text{(B6)}$$

and reassigning the names of the remaining variables according to $(\mathbf{r}_0,\mathbf{r}_2,\ldots,\mathbf{r}_{p-2},\mathbf{r}_p)\Rightarrow(\mathbf{r}_0,\mathbf{r}_1,\ldots,\mathbf{r}_{p/2-1},\mathbf{r}_{p/2})$, we find

$$Z_1(d;A,B,N)=Z_1(d;A(\pi/2B)^{(3/2)2^{N-1}},B/2,N-1). \quad \text{(B7)}$$

Denoting the original parameters A and B by A_N and B_N, we may rewrite this as

$$Z_1(d;A_N,B_N,N)=Z_1(d;A_{N-1},B_{N-1},N-1), \quad \text{(B8)}$$

where

$$A_{N-1}=A_N\left[\left(\frac{2\pi}{2B_N}\right)^{(3/2)}\right]^{2^{N-1}}, \quad B_{N-1}=\frac{B_N}{2}. \quad \text{(B9)}$$

This can be repeated, and after N cycles we have integrated over $2^{N-1}+2^{N-2}+\cdots+1=2^N-1$ bead positions, i.e., all the movable beads. The final result is then

$$Z_1(d)=A_0\exp(-B_0(\mathbf{r}_P-\mathbf{r}_0)^2)=A_0\exp(-B_0d^2), \quad \text{(B10)}$$

where

$$B_0=\frac{B_N}{2^N}=\frac{B_N}{P}=\frac{m}{2\hbar^2\beta} \quad \text{(B11)}$$

is independent of P. A_0 may also be evaluated, but its value does not affect the final result. We get, using Eq. (B5),

$$F_K^{(1)}(d)=-k_BT\ln\left(\frac{Z_1(d)}{Z_1(0)}\right)=(k_BT)^2md^2/(2\hbar^2). \quad \text{(B12)}$$

2. Calculation of $F_K^{(2)}$

$F_K^{(2)}$ is the free-energy difference between two distributions of the polymer chain, both with the two end beads fixed at a distance d between them, with and without the potential barrier. We start from the partition function written with a scaled potential $\lambda V(\mathbf{r})$,

$$Z_2(\lambda)=\int d\mathbf{r}_1\int d\mathbf{r}_2\cdots\int d\mathbf{r}_{P-1}\times\exp\left[-\left(\frac{\beta}{P}\right)\sum_{i=1}^{P}\left(\frac{m(\mathbf{r}_i-\mathbf{r}_{i-1})^2}{2(\hbar\beta/P)^2}+\lambda V(\mathbf{r}_i)\right)\right]. \quad \text{(B13)}$$

The free energy for creating the potential barrier $V(\mathbf{r})$ is

$$F_K^{(2)}=\int_0^1 d\lambda\left\langle\frac{\partial E}{\partial\lambda}\right\rangle_\lambda, \quad \text{(B14)}$$

where

$$E(\lambda)=E(\{\mathbf{r}_i\},\lambda)=\sum_{i=1}^{P}\left(\frac{Pm}{2\hbar^2\beta^2}(\mathbf{r}_i-\mathbf{r}_{i-1})^2+\frac{1}{P}\lambda V(\mathbf{r}_i)\right), \quad \text{(B15)}$$

$$\frac{\partial E}{\partial\lambda}=\frac{1}{P}\sum_i V(\mathbf{r}_i), \quad \text{(B16)}$$

and where $\langle\ \rangle_\lambda$ denotes averaging with respect to the probability distribution

$$P_\lambda(\{\mathbf{r}_i\})=\frac{\exp\left[-\beta\sum_{i=1}^{P}\left(\frac{Pm}{2\hbar^2\beta^2}(\mathbf{r}_i-\mathbf{r}_{i-1})^2+\frac{\lambda}{P}V(\mathbf{r}_i)\right)\right]}{Z_2(\lambda)}. \quad \text{(B17)}$$

So we have

$$F_K^{(2)}=\int_0^1 d\lambda\int d\mathbf{r}_1\cdots d\mathbf{r}_{P-1}\left(\frac{1}{P}\sum_i V(\mathbf{r}_i)\right)P_\lambda(\{\mathbf{r}_i\}). \quad \text{(B18)}$$

Expression (7) is a coarse-grained version of this result.

[1] R. A. Marcus, J. Chem. Phys. **24**, 966 (1956); 979 (1956).
[2] D. N. Beratan, J. N. Betts, and J. N. Onuchic, Science **252**, 1285 (1991).
[3] A. Mosyak, P. Graf, I. Benjamin, and A. Nitzan, J. Phys. Chem. A **101**, 429 (1997).
[4] I. Benjamin, D. Evans, and A. Nitzan, J. Chem. Phys. **106**, 6647 (1997); 1291 (1997).
[5] A. Nitzan and I. Benjamin, Acc. Chem. Res. **32**, 854 (1999).
[6] M. Galperin, A. Nitzan, and I. Benjamin, J. Phys. Chem. A **106**, 10790 (2002).
[7] K. S. Schweizer, R. M. Stratt, D. Chandler, and P. G. Wolynes, J. Chem. Phys. **75**, 1347 (1981); D. Chandler and P. G. Wolynes, *ibid.* **74**, 4078 (1981).
[8] M. Marchi and D. Chandler, J. Chem. Phys. **95**, 889 (1991).
[9] A. Kuki and P. G. Wolynes, Science **236**, 1647 (1987).
[10] M. J. Gillan, Philos. Mag. A **58**, 257 (1988); G. A. Voth, D. Chandler, and W. H. Miller, J. Chem. Phys. **91**, 7749 (1989).
[11] J. Bardeen, Phys. Rev. Lett. **6**, 57 (1961); M. Galperin, D. Segal, and A. Nitzan, J. Chem. Phys. **111**, 1569 (1999).
[12] P. J. Rossky and J. Schnitker, J. Chem. Phys. **86**, 3642 (1987).
[13] M. Galperin, S. Toledo, and A. Nitzan, J. Chem. Phys. **117**, 10817 (2002).